Structural Features for Functional Selectivity at Serotonin Receptors

Daniel Wacker *et al.*

Science **340**, 615 (2013);
DOI: 10.1126/science.1232808

Science (print ISSN 0036-8075; online ISSN 1095-9203) is published weekly, except the last week in December, by the American Association for the Advancement of Science, 1200 New York Avenue NW, Washington, DC 20005.

Structural Features for Functional Selectivity at Serotonin Receptors

Daniel Wacker,[1] Chong Wang,[1] Vsevolod Katritch,[1] Gye Won Han,[1] Xi-Ping Huang,[2] Eyal Vardy,[2] John D. McCorvy,[2] Yi Jiang,[1,3] Meihua Chu,[1] Fai Yiu Siu,[1] Wei Liu,[1] H. Eric Xu,[3,4] Vadim Cherezov,[1] Bryan L. Roth,[2]* Raymond C. Stevens[1]*

Drugs active at G protein–coupled receptors (GPCRs) can differentially modulate either canonical or noncanonical signaling pathways via a phenomenon known as functional selectivity or biased signaling. We report biochemical studies showing that the hallucinogen lysergic acid diethylamide, its precursor ergotamine (ERG), and related ergolines display strong functional selectivity for β-arrestin signaling at the 5-HT_{2B} 5-hydroxytryptamine (5-HT) receptor, whereas they are relatively unbiased at the 5-HT_{1B} receptor. To investigate the structural basis for biased signaling, we determined the crystal structure of the human 5-HT_{2B} receptor bound to ERG and compared it with the 5-HT_{1B}/ERG structure. Given the relatively poor understanding of GPCR structure and function to date, insight into different GPCR signaling pathways is important to better understand both adverse and favorable therapeutic activities.

Apart from canonical G protein–mediated signaling, G protein–coupled receptors (GPCRs) also activate noncanonical G protein–independent pathways, frequently mediated by β-arrestins (*1*, *2*). So-called "biased" GPCR agonists differentially activate signaling pathways with distinct efficacies and potencies as compared with unbiased agonists that activate both pathways equally (*3*). This preferential activation of one pathway over the other has been termed "functional selectivity" or "signaling bias" (*2*–*5*). Depending on the receptor, biased signaling patterns are key for mediating inflammation (*6*), apoptosis (*7*), and many other processes (*2*). Biased ligands have been proposed to stabilize receptor conformations that are distinct from those induced by unbiased ligands and selectively change the propensity of GPCR coupling to either G proteins or β-arrestins (*2*).

Agonist-induced changes in trigger motifs of GPCRs (*8*) near the binding pocket facilitate large-scale helical movements that are accompanied by rearrangements in highly conserved residues called "microswitches" (*9*) that prime GPCRs for subsequent G protein binding and activation (*10*). The structural features of a signaling-biased receptor state remain elusive, and although complexes of two β-arrestin–biased ligands with the β_1-adrenergic receptor (β_1AR) have recently been solved (*11*), they did not reveal activation-related changes in the receptor.

To elucidate molecular and structural details of biased signaling, we characterized G protein– and β-arrestin–mediated signaling at G protein–coupled serotonin [5-hydroxytryptamine (5-HT)] receptors with several representative ergolines, such as lysergic acid diethylamide (LSD) and ergotamine (ERG). Additionally, we solved the crystal structure of the 5-HT_{2B} receptor in complex with ERG, which was identified as a highly biased agonist for the 5-HT_{2B} receptor (*12*).

To investigate potential differences of ergoline signaling at 5-HT receptors, we examined three prototypical serotonin receptors that interact with distinct G proteins. The 5-HT_{1B} receptor inhibits cyclic adenosine monophosphate (cAMP) production through G_i, the 5-HT_{2B} receptor mediates phospholipase C activation through G_q, and the 5-HT_{7A} receptor stimulates cAMP production through G_s (*13*). We compared G protein– and β-arrestin–mediated signaling at cloned human 5-HT_{1B} and 5-HT_{2B} receptors and G protein–mediated signaling at 5-HT_{7A} receptors stimulated by selective and nonselective ligands in human embryonic kidney (HEK) 293 cells (Fig. 1 and table S1) (*14*).

LSD and, especially, ERG displayed bias for β-arrestin signaling at 5-HT_{2B} (bias factors 101 and 228, respectively) (Fig. 1D), minimal bias at 5-HT_{1B} (bias factors 5 and 25, respectively) (Fig. 1D), and G protein antagonism at 5-HT_{7A} receptors (Fig. 1B and table S1). We also found significant β-arrestin signaling bias for other ergolines—such as dihydroergotamine (DHE), methylergonovine (MTE), pergolide (PER), and cabergoline (CAB)—at the 5-HT_{2B} receptor, whereas all other evaluated compounds showed no significant bias (Fig. 1D). ERG and DHE, both of which contain a large tripeptide moiety substitution at the amide scaffold, displayed more extreme signaling bias at the 5-HT_{2B} receptor compared with LSD.

To investigate the molecular details responsible for biased signaling, we crystallized an engineered 5-HT_{2B} receptor construct in complex with ERG, solved its structure at 2.7 Å (fig. S1 and S2 and table S3), and compared it with the structure of 5-HT_{1B}/ERG reported in the companion manuscript (*15*), as well as to other known unbiased active-state GPCR structures. Residues $P^{5.50}$, $I^{3.40}$, and $F^{6.44}$ (*16*, *17*), the "P-I-F" motif (P, Pro; I, Ile; F, Phe), form an interface between helices V, III, and VI near the base of the ligand binding pocket in β_2AR and many other aminergic receptors, including all 5-HT GPCRs. In the active-state structures of β_2AR (*8*, *18*), a chain of conformational rearrangements occurs in the P-I-F residues, in which an inward shift of helix V residue $P211^{5.50}$ is coupled with: (i) a rotamer switch in $I121^{3.40}$, (ii) a large movement of the $F282^{6.44}$ side chain, and (iii) a corresponding rotation of helix VI on the cytoplasmic side (*8*). The 5-HT_{1B} and 5-HT_{2B} receptor structures display two different conformations of the P-I-F motif (Fig. 2). For the 5-HT_{1B} receptor, we observe that the P-I-F configuration is essentially identical to that of the active-state of β_2AR [β_2AR-R*, Protein Data Bank identification number (PDB ID): 3SN6 (*18*)] (Fig. 2B). Whereas the 5-HT_{2B} receptor adopts a similar active-like conformation of $P229^{5.50}$ and $I143^{3.40}$, the side-chain conformation of $F333^{6.44}$ was similar to that observed in the inactive β_2AR [β_2AR-R, PDB ID: 2RH1 (*19*)] (Fig. 2C and fig. S2B). The P-I-F motif, therefore, appears to be in an active-like conformation in the 5-HT_{1B} structure, but only in an intermediate active conformation in the 5-HT_{2B} receptor structure.

At the cytoplasmic side of the receptors, GPCR activation is generally characterized by the displacement of helices V, VI, and VII (*10*). The magnitude of the helical motions depends on the activation-state; for example, the outward displacement of the intracellular tip of helix VI ranges between 3 and 14 Å, whereas helix VII shifts between 3 to 5 Å toward the receptor core (*10*, *18*–*22*). These concerted rearrangements induce an opening of the helical bundle at the cytoplasmic side, which facilitates the binding and subsequent activation of G proteins. Analysis of the 5-HT_{1B} and 5-HT_{2B} receptor structures shows that the conformation in the intracellular half of the helical bundle is notably shifted toward that seen in active-state GPCR structures (Fig. 3 and figs. S3 and S4) and is distinct from those of inactive-state GPCR structures (Fig. 3 and figs. S5 and S6). In the 5-HT_{1B} and 5-HT_{2B} receptor structures, the helix VI intracellular part is located at least 2 to 4 Å further away from the receptor core than in the inactive-state structures of other aminergic GPCRs (fig. S5). This conformation of helix VI is close to the one observed in active-state structures of the A_{2A} adenosine receptor (A_{2A}AR) (fig. S3) and rhodopsin (Rho) (fig. S4), though the outward shift of the helix is smaller in magnitude compared with that of the G protein–bound β_2AR (Fig. 3, A and C). The only difference that we observed in helix VI between 5-HT receptor subtypes was a small clockwise rotation in the 5-HT_{1B} receptor toward the active state that is

[1]Department of Integrative Structural and Computational Biology, The Scripps Research Institute, 10550 North Torrey Pines Road, La Jolla, CA 92037, USA. [2]National Institute of Mental Health Psychoactive Drug Screening Program, Department of Pharmacology and Division of Chemical Biology and Medicinal Chemistry, University of North Carolina Chapel Hill Medical School, Chapel Hill, NC 27599, USA. [3]Van Andel Research Institute/Shanghai Institute of Materia Medica Center, CAS-Key Laboratory of Receptor Research, Shanghai Institute of Materia Medica, Chinese Academy of Sciences, Shanghai, China. [4]Laboratory of Structural Sciences, Van Andel Research Institute, 333 Bostwick Ave NE, Grand Rapids, MI 49503, USA.

*Corresponding author. E-mail: bryan_roth@med.unc.edu (B.L.R.); stevens@scripps.edu (R.C.S.)

absent in the 5-HT$_{2B}$ structure (Figs. 2, B and C, and 3, A and C). Helix VII in both 5-HT receptor structures also displays intermediate active states when compared with β_2AR (Fig. 3, B and D), where it is shifted toward the receptor core as compared with inactive-state structures of other aminergic GPCRs (fig. S6). Whereas the 5-HT$_{2B}$/ERG receptor structure shows less pronounced active-like changes in helix VI, helix VII appears to be in a more active conformation than it is in the 5-HT$_{1B}$/ERG receptor structure (Fig. 3, B and D).

Another important aspect of GPCR activation is the rearrangement of side chains in highly conserved motifs D(E)/RY (helix III) and NPxxY (helix VII) (D, Asp; E, Glu; R, Arg; Y, Tyr; N, Asn; x, any amino acid), which are referred to as microswitches (*9*). Thus, the D(E)/RY motif

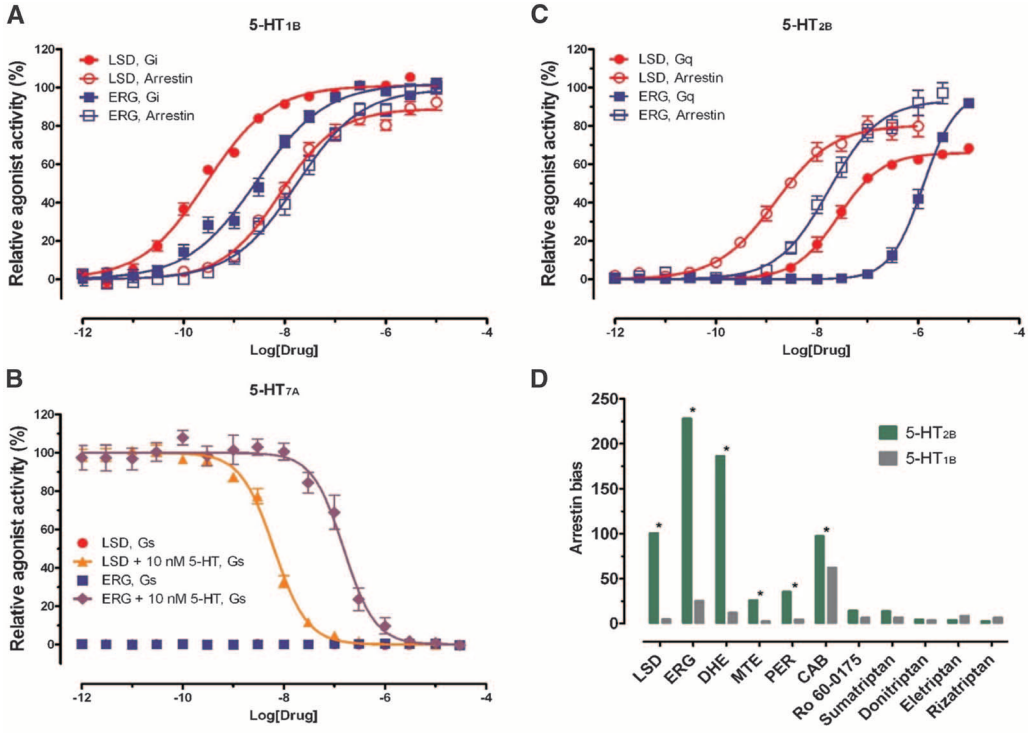

Fig. 1. Distinct signaling properties of LSD and ERG at 5-HT$_{1B}$, 5-HT$_{7A}$, and 5-HT$_{2B}$ receptors. We used luminescence-based assays to measure 5-HT$_{1B}$ receptor–mediated G_i activation and cAMP production, fluorescence-based calcium mobilization assays to measure 5-HT$_{2B}$ receptor–mediated G_q activation, and β-arrestin translocation-dependent luciferase reporter assays to measure 5-HT$_{1B}$ and 5-HT$_{2B}$ receptor–mediated β-arrestin recruitment, all in HEK293 derived cells. (**A**) Normalized concentration-response studies for LSD and ERG at human cloned 5-HT$_{1B}$ receptor–mediated activation of G_i and noncanonical (arrestin) signaling. (**B**) Normalized concentration-response studies for LSD and ERG at human cloned 5-HT$_{7A}$ receptor–mediated activation of G_s signaling in the presence and absence of 5-HT. The solid red circles for LSD-G_s signals are superimposed by the solid blue squares for ERG-G_s signals and, thus, not visible. (**C**) Normalized concentration-response studies for LSD and ERG at human cloned 5-HT$_{2B}$ receptor–mediated activation of G_q and noncanonical (arrestin) signaling. (**D**) Mean β-arrestin bias factors were calculated for serotonergic agonists at 5-HT$_{2B}$ and 5-HT$_{1B}$ receptors. Concentration-responses curves were fit to the Black and Leff operational model to obtain transduction coefficients [Log(τ/K_A)] (where τ is agonist efficacy and K_A is the equilibrium dissociation constant) for each ligand at each corresponding pathway. The ΔLog(τ/K_A) was then calculated with 5-HT as a reference agonist for each pathway, and the $\Delta\Delta$Log(τ/K_A) was calculated between two pathways for each ligand. The bias factor is unitless and defined as $10^{\Delta\Delta\text{Log }\tau/K_A}$ (*28*). Compounds with values close to one represent unbiased agonists, whereas compounds with large numerical values, typically >100, represent extremely biased agonists. *$P <$ 0.0001 via two-way analysis of variance comparing 5-HT$_{2B}$ versus 5-HT$_{1B}$ bias factors; n = 3 to 6 separate experiments. ERG, DHE, and, to a lesser extent, LSD, MTE, and PER show strong β-arrestin bias at the 5-HT$_{2B}$ receptor, but not the 5-HT$_{1B}$ receptor. Error bars in (A) to (C) denote SEM from a minimum of three assays.

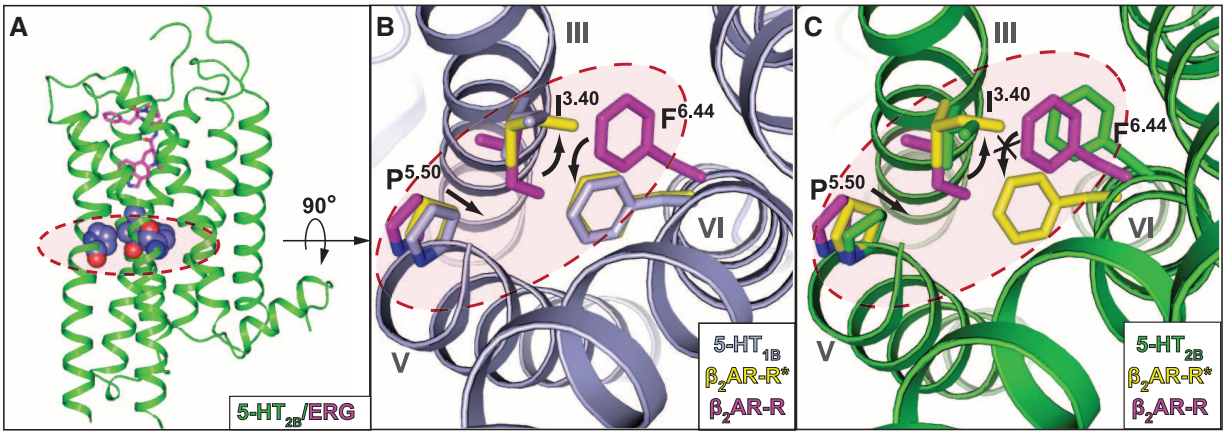

Fig. 2. Trigger motif P-I-F displays active and intermediate active states for 5-HT$_{1B}$ and 5-HT$_{2B}$ receptors, respectively. Residues of the P-I-F motif are highlighted in a dashed red circle in each panel. (**A**) Overall architecture of the 5-HT$_{2B}$ receptor (green) bound to ERG (magenta); residues of the $P^{5.50}$ $I^{3.40}$ $F^{6.44}$ motif are illustrated in space-filling representation. (**B**) Alignment between 5-HT$_{1B}$ receptor (gray), β_2AR-R (magenta; PDB ID: 2RH1), and β_2AR-R*(yellow; PDB ID: 3SN6) indicates an activated P-I-F motif in the 5-HT$_{1B}$/ERG structure. Black arrows denote likely rearrangements upon 5-HT$_{1B}$ receptor activation, according to analysis of β_2AR. (**C**) Alignment between 5-HT$_{2B}$ receptor (green), β_2AR-R (magenta), and β_2AR-R* (yellow) suggests an intermediate active state of the P-I-F motif in the 5-HT$_{2B}$/ERG structure, with $F^{6.44}$ in an inactive conformation. Black arrows indicate likely rearrangements upon 5-HT$_{2B}$ receptor activation, according to analysis of β_2AR.

of all inactive-state and most active-state GPCR structures shows an intact salt bridge between the side chains of D(E)$^{3.49}$ and R$^{3.50}$. Importantly, this salt bridge is broken only in the active-state structures of β_2AR-G$\alpha\beta\gamma$ (*18*) and Opsin-GαCT (*21*), where R$^{3.50}$ interacts instead with the G protein and Gα peptide, respectively. The salt bridge is preserved between the side chains of R153$^{3.50}$ and D152$^{3.49}$ in the 5-HT$_{2B}$ receptor structure, but it is broken in the 5-HT$_{1B}$ receptor structure (Fig. 4, A, B, and D; and fig. S2C). In the 5-HT$_{1B}$ receptor structure, the D146$^{3.49}$ side chain forms a hydrogen bond to Y157 in intracellular loop 2, and the R147$^{3.50}$ side chain interacts with the main-chain carbonyl in a loop of the fusion protein BRIL (residue L1048; L, Leu), which is partially inserted into the G protein binding crevice (Fig. 4A). Thus, the conformation of the D(E)RY motif mimics the active state of β_2AR in the 5-HT$_{1B}$ structure but resembles the inactive state in the 5-HT$_{2B}$ structure (Fig. 4, A and C; and fig. S7).

The highly conserved NPxxY motif at the cytoplasmic end of helix VII is another key microswitch of GPCR activation (*9*). Upon GPCR activation, the intracellular end of helix VII moves toward the receptor core, and a rotation of Y$^{7.53}$ around the helical axis moves the side chain further into the seven-transmembrane (TM) bundle (*10*). Both 5-HT receptor structures show active-state conformations of the NPxxY motif when compared with β_2AR, A$_{2A}$AR, and Rho (Fig. 4, D and E; and figs. S2D and S7), with more pronounced activation features in the 5-HT$_{2B}$ receptor.

Our analysis indicates that the 5-HT$_{1B}$/ERG structure has most of the attributes of a classical agonist-induced, active-like state, consistent with our biochemical findings that ERG is a comparatively unbiased agonist at the 5-HT$_{1B}$ receptor. In contrast, the 5-HT$_{2B}$/ERG structure exhibits conformational characteristics of both the active and inactive states. The structure of β_2AR-G$\alpha\beta\gamma$ complex, along with recent nuclear magnetic resonance and fluorescence studies of β_2AR, implicates helix VI predominantly in G protein signaling, whereas conformational changes in helix VII are associated with enhanced β-arrestin signaling (*18*, *23*, *24*). Thus, an active-like state in the helix VII conformation of the 5-HT$_{2B}$ receptor, but only partial changes in helix VI, mirrors the strong β-arrestin bias of ERG at 5-HT$_{2B}$ receptors observed in pharmacological assays.

A likely structural explanation for the distinct conformational features and biased pharmacology of ERG between 5-HT$_{1B}$ and 5-HT$_{2B}$ receptors can be found in the region of the extracellular loop 2 (ECL2) junction with helix V. In the 5-HT$_{2B}$ receptor structure, E212-R213-F214 forms an additional helical turn stabilized by a structured water molecule at the extracellular tip of helix V (Fig. 5). As a result, the segment of ECL2 that connect helices III and V via the conserved disulfide bond is shortened in the 5-HT$_{2B}$ receptor, inducing an inward shift and creating a conformational constraint on the position of the extracellular tip of helix V. Because of these rearrangements, ERG forms additional hydrophobic contacts with M218$^{5.39}$, L347$^{6.58}$, V348$^{6.59}$, L362$^{7.35}$, and K211^{ECL2} (M, Met; V, Val; K, Lys) (fig. S8A) and stabilizes a closer distance between helices V and VI, which form hydrophobic contacts between L219$^{5.40}$, V348$^{6.59}$, and L349$^{6.60}$, along with a hydrogen bond between S222$^{5.43}$ and N344$^{6.55}$ (S, Ser) (fig. S8B). These extensive ligand-mediated interactions between helices V and VI in the 5-HT$_{2B}$/ERG complex may be inferred to prevent rearrangements in helix VI and the corresponding rotation of F$^{6.44}$ (*8*), observed in the 5-HT$_{1B}$ receptor and structures of other active-state GPCRs. The strengthened interactions of helix V and VI through ligand-mediated hydrogen bonds to both helices have also been linked to inhibition of G protein signaling at β_2AR by the most efficacious inverse agonist (*25*).

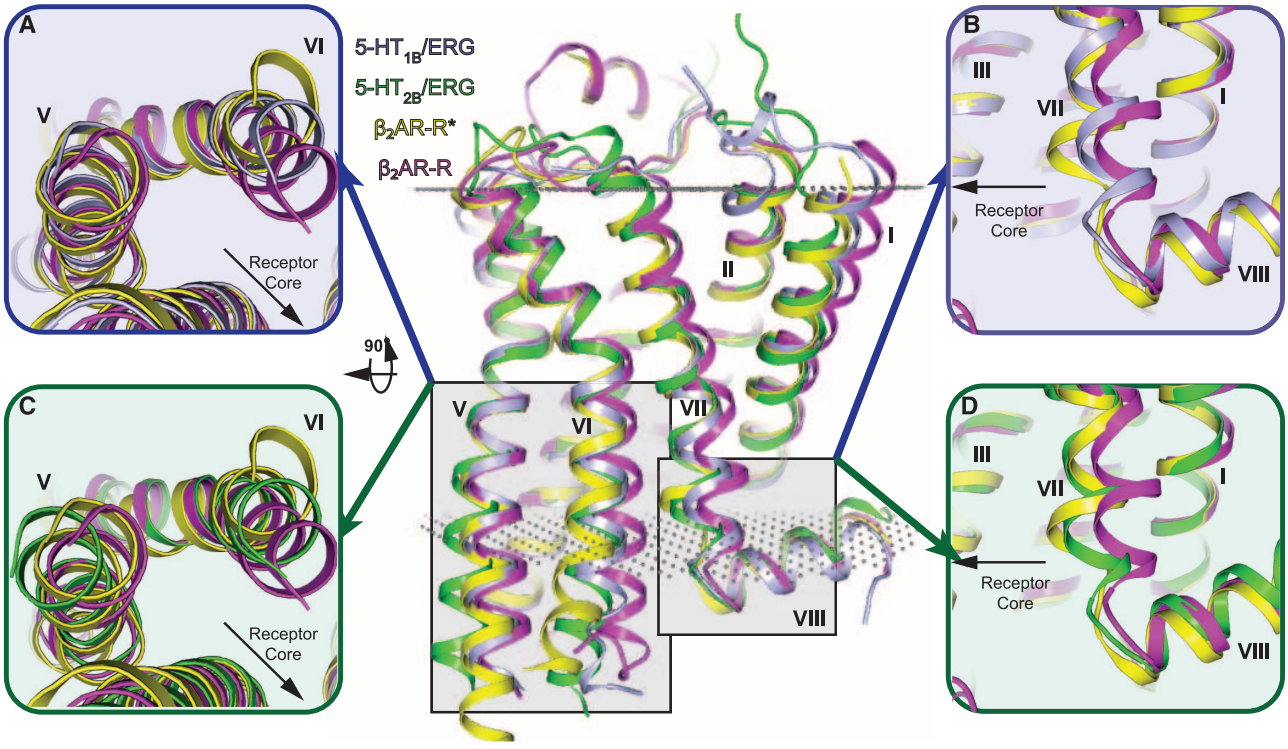

Fig. 3. Structural alignment with β_2AR-R and β_2AR-R* reveals distinct active-state seven-TM conformations of the 5-HT$_{1B}$ and 5-HT$_{2B}$ receptor structures. All structures were analyzed based on the last membrane-embedded residue to minimize the effect of G proteins and fusion partners on the relative helix positions (see supplementary materials). The center panel shows the overall seven-TM configuration of β_2AR-R (magenta; PDB ID: 2RH1), β_2AR-R*(yellow; PDB ID: 3SN6), 5-HT$_{1B}$ (gray), and 5-HT$_{2B}$ (green) receptors aligned through helices I to IV. Membrane boundaries are indicated by gray dots according to the Orientations of Proteins in Membranes database (*29*). (**A** and **C**) Intracellular view of helices V and VI in β_2AR-R, β_2AR-R* compared with (A) the 5-HT$_{1B}$ receptor or (C) the 5-HT$_{2B}$ receptor. Residues on the intracellular side of the membrane have been removed for better comparison of ligand-induced helical rearrangements (see main text). Helix VI of the 5-HT$_{1B}$ and 5-HT$_{2B}$ receptors is in an intermediate active state compared with β_2AR. (**B** and **D**) Side view of helices VII and VIII in β_2AR-R, β_2AR-R* and the (B) 5-HT$_{1B}$ receptor or (D) 5-HT$_{2B}$ receptor. Helix VII of the 5-HT$_{1B}$ and 5-HT$_{2B}$ receptors is in an intermediate active state compared with β_2AR, with more pronounced activation features for the 5-HT$_{2B}$ receptor.

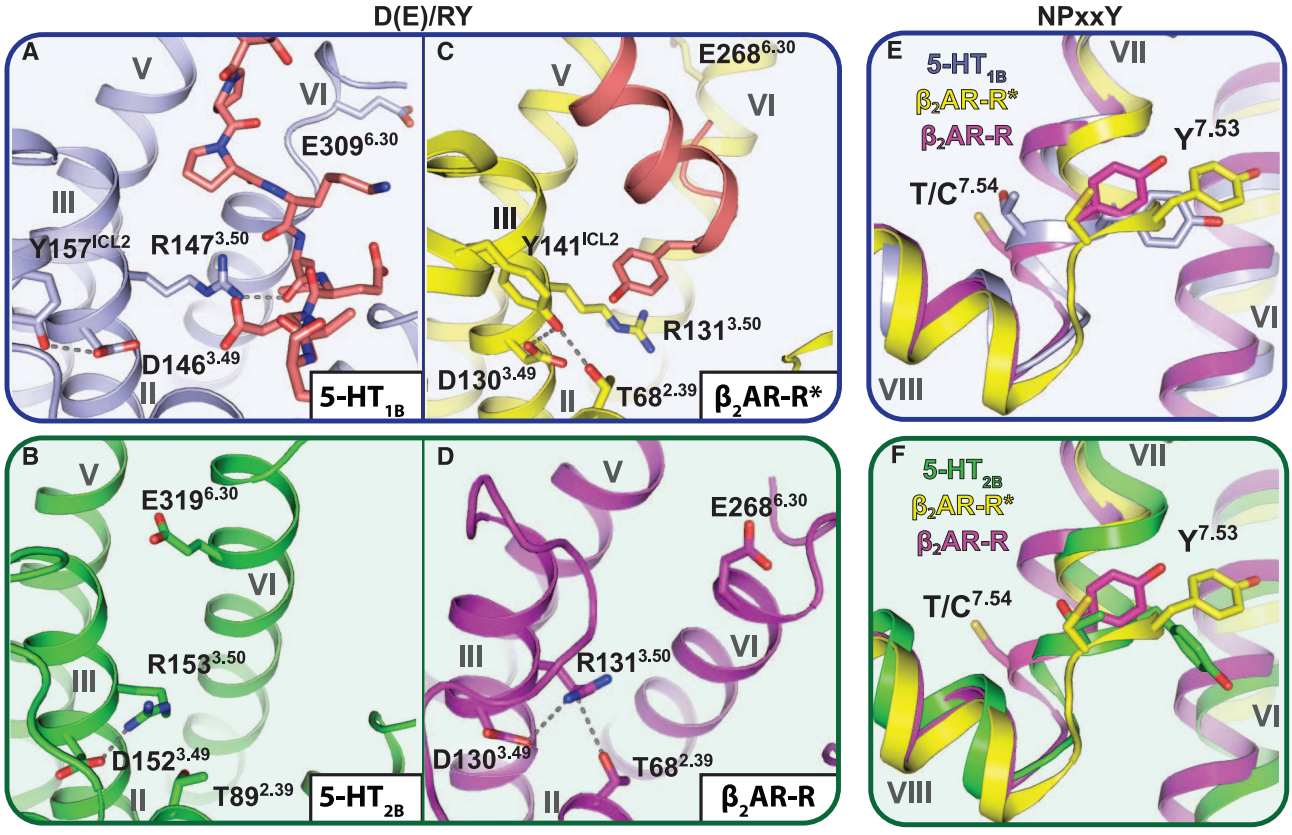

Fig. 4. Activation state of the D(E)/RY and NPxxY motifs in 5-HT$_{1B}$ and 5-HT$_{2B}$ receptors compared with β_2AR-R and β_2AR-R*. Configuration of the D(E)/RY motif in (**A**) the 5-HT$_{1B}$ receptor (gray), (**B**) the 5-HT$_{2B}$ receptor (green), (**C**) β_2AR-R* (yellow; PDB ID: 3SN6), and (**D**) β_2AR-R (magenta; PDB ID: 2RH1). Residues of the G protein in β_2AR-R* (C) and the G protein–mimicking BRIL loop (A) are highlighted in orange. The conformation of the D(E)/RY motif in the 5-HT$_{1B}$ receptor is similar to that observed in β_2AR-R*, whereas the configuration of the 5-HT$_{2B}$ receptor compares to that of β_2AR-R. (**E** and **F**) Conformational states of $Y^{7.53}$ of the NPxxY motif and the proceeding residue 7.54 in β_2AR-R, β_2AR-R*, and (E) the 5-HT$_{1B}$ receptor or (F) 5-HT$_{2B}$ receptor. When compared with β_2AR, the conformation of the NPxxY motif in the 5-HT$_{1B}$ receptor is in an intermediate active state, whereas the configuration of the 5-HT$_{2B}$ receptor is similar to β_2AR-R*. T, Thr; C, Cys.

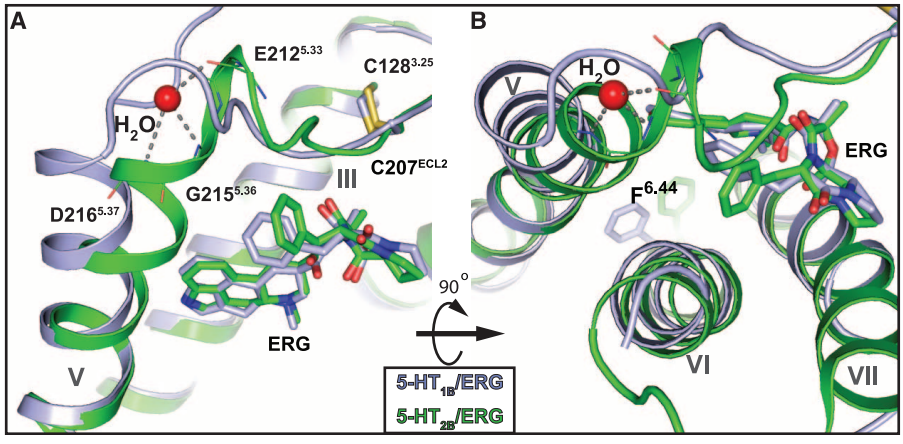

Fig. 5. Structural differences in extracellular configuration of helix V between 5-HT$_{1B}$ and 5-HT$_{2B}$ receptors likely explain β-arrestin functional selectivity at the 5-HT$_{2B}$ receptor. Side view (**A**) and top view (**B**) of 5-HT$_{1B}$ (gray) and 5-HT$_{2B}$ (green) receptors show a kink in the extracellular end of helix V in the 5-HT$_{2B}$ receptor. A water molecule (red sphere) was found to stabilize the kink through hydrogen bonds (gray dashed lines) with the $E212^{5.33}$ main-chain carbonyl oxygen and the main-chain nitrogens of $D216^{5.37}$ and $G215^{5.36}$ (G, Gly). Main-chain atoms of both residues are shown as lines.

Ergolines predominantly signal through β-arrestin pathways at 5-HT$_{2B}$ receptors, whereas signaling at 5-HT$_{1B}$ receptors appears nonbiased. The differential signaling patterns are mirrored in the crystal structures, which show features of an intermediate active state for the 5-HT$_{1B}$ receptor and a β-arrestin–biased activation state for the 5-HT$_{2B}$ receptor. We propose a mechanism by which ERG stabilizes a conformation of the 5-HT$_{2B}$ receptor that selectively interferes with G protein signaling (fig. S9). The tripeptide moiety of ERG appears to interfere with G protein signaling at the 5-HT$_{2B}$ receptor, as ERG exhibits strongly increased β-arrestin signaling bias compared with LSD and MTE. Because both therapeutic (*26*) and adverse (*27*) drug effects have been associated with β-arrestin recruitment by GPCRs, identifying the features of biased GPCR states by known and yet to be discovered intracellular signaling proteins may facilitate the development of safer and more effective therapeutics with selective signaling profiles.

References and Notes

1. L. M. Luttrell *et al.*, *Science* **283**, 655 (1999).
2. E. Reiter, S. Ahn, A. K. Shukla, R. J. Lefkowitz, *Annu. Rev. Pharmacol. Toxicol.* **52**, 179 (2012).
3. T. Kenakin, *J. Pharmacol. Exp. Ther.* **336**, 296 (2011).
4. J. A. Allen, B. L. Roth, *Annu. Rev. Pharmacol. Toxicol.* **51**, 117 (2011).
5. J. D. Urban *et al.*, *J. Pharmacol. Exp. Ther.* **320**, 1 (2007).
6. H. Gao *et al.*, *Mol. Cell* **14**, 303 (2004).
7. S. Ahn, J. Kim, M. R. Hara, X. R. Ren, R. J. Lefkowitz, *J. Biol. Chem.* **284**, 8855 (2009).

8. S. G. Rasmussen *et al.*, *Nature* **469**, 175 (2011).
9. R. Nygaard, T. M. Frimurer, B. Holst, M. M. Rosenkilde, T. W. Schwartz, *Trends Pharmacol. Sci.* **30**, 249 (2009).
10. V. Katritch, V. Cherezov, R. C. Stevens, *Annu. Rev. Pharmacol. Toxicol.* **53**, 531 (2013).
11. T. Warne, P. C. Edwards, A. G. Leslie, C. G. Tate, *Structure* **20**, 841 (2012).
12. X. P. Huang *et al.*, *Mol. Pharmacol.* **76**, 710 (2009).
13. M. Berger, J. A. Gray, B. L. Roth, *Annu. Rev. Med.* **60**, 355 (2009).
14. Materials and methods and supplementary figures and tables are available as supplementary materials on *Science* Online.
15. C. Wang *et al.*, *Science* **340**, 610 (2013).
16. Superscripts refer to the Ballesteros-Weinstein numbering, in which the most conserved among class A GPCRs residues in each TM helix are designated x.50, where x is the helix number.
17. J. A. Ballesteros, H. Weinstein, *Methods Neurosci.* **25**, 366 (1995).
18. S. G. Rasmussen *et al.*, *Nature* **477**, 549 (2011).
19. V. Cherezov *et al.*, *Science* **318**, 1258 (2007).
20. Y. Imamoto, M. Kataoka, F. Tokunaga, K. Palczewski, *Biochemistry* **39**, 15225 (2000).
21. P. Scheerer *et al.*, *Nature* **455**, 497 (2008).
22. F. Xu *et al.*, *Science* **332**, 322 (2011).
23. J. J. Liu, R. Horst, V. Katritch, R. C. Stevens, K. Wüthrich, *Science* **335**, 1106 (2012).
24. R. Rahmeh *et al.*, *Proc. Natl. Acad. Sci. U.S.A.* **109**, 6733 (2012).
25. D. Wacker *et al.*, *J. Am. Chem. Soc.* **132**, 11443 (2010).
26. J. A. Allen *et al.*, *Proc. Natl. Acad. Sci. U.S.A.* **108**, 18488 (2011).
27. A. K. Finn, J. L. Whistler, *Neuron* **32**, 829 (2001).
28. T. Kenakin, C. Watson, V. Muniz-Medina, A. Christopoulos, S. Novick, *ACS Chem. Neurosci.* **3**, 193 (2012).
29. M. A. Lomize, I. D. Pogozheva, H. Joo, H. I. Mosberg, A. L. Lomize, *Nucleic Acids Res.* **40**, D370 (2012).

Acknowledgments: This work was supported by the National Institute of General Medical Sciences (NIGMS) Protein Structure Initiative:Biology grant U54 GM094618 for biological studies and structure production (target GPCR-4) (V.K., V.C., and R.C.S.); NIH Common Fund in Structural Biology grant P50 GM073197 for technology development (V.C. and R.C.S.); the Jay and Betty Van Andel Foundation, Amway (China), grant R01 DK071662; Ministry of Science and Technology (China) grants 2012ZX09301001-005 and 2012CB910403 (H.E.X.); grants U19 MH82441, R01 MH61887, and the National Institute of Mental Health Psychoactive Drug Screening Program (X.-P.H., E.V., and B.L.R.); and the Michael Hooker Chair of Pharmacology (B.L.R.). D.W. is supported by a Boehringer Ingelheim Fonds Ph.D. Fellowship. R.C.S. is a founder and paid consultant for Receptos, a GPCR structure–based drug discovery company. We thank J. Velasquez for help on molecular biology; T. Trinh, K. Allin, and M. Chu for help on baculovirus expression; L. N. Collins for help on initial construct selection; K. Kadyshevskaya for assistance with figure preparation; A. Walker for assistance with manuscript preparation; I. Wilson for careful review and scientific feedback on the manuscript; T. Kenakin (University of North Carolina) for helpful discussions regarding the quantification of ligand bias; J. Smith, R. Fischetti, and N. Sanishvili for assistance in development and use of the minibeam and beamtime at GM/CA-CAT beamline 23-ID at the Advanced Photon Source, which is supported by National Cancer Institute grant Y1-CO-1020 and NIGMS grant Y1-GM-1104. Use of the Advanced Photon Source was supported by the Office of Science of the U.S. Department of Energy. Coordinates and the structure factors of the 5-HT_{2B}/ERG complex have been deposited in the Protein Data Bank under the accession code 4IB4.

Supplementary Materials

www.sciencemag.org/cgi/content/full/science.1232808/DC1
Materials and Methods
Figs. S1 to S9
Tables S1 to S3
References (*30*–*42*)

15 November 2012; accepted 27 February 2013
Published online 21 March 2013;
10.1126/science.1232808

R-Loop Stabilization Represses Antisense Transcription at the *Arabidopsis FLC* Locus

Qianwen Sun,[1] Tibor Csorba,[1] Konstantina Skourti-Stathaki,[2] Nicholas J. Proudfoot,[2] Caroline Dean[1]*

Roles for long noncoding RNAs (lncRNAs) in gene expression are emerging, but regulation of the lncRNA itself is poorly understood. We have identified a homeodomain protein, AtNDX, that regulates *COOLAIR*, a set of antisense transcripts originating from the 3′ end of *Arabidopsis FLOWERING LOCUS C* (*FLC*). AtNDX associates with single-stranded DNA rather than double-stranded DNA non–sequence-specifically in vitro, and localizes to a heterochromatic region in the *COOLAIR* promoter in vivo. Single-stranded DNA was detected in vivo as part of an RNA-DNA hybrid, or R-loop, that covers the *COOLAIR* promoter. R-loop stabilization mediated by AtNDX inhibits *COOLAIR* transcription, which in turn modifies *FLC* expression. Differential stabilization of R-loops could be a general mechanism influencing gene expression in many organisms.

A major factor determining natural variation in flowering in *Arabidopsis* is quantitative variation in the expression and silencing of the floral repressor gene *FLC* (*1*, *2*). Multiple pathways regulate *FLC*, and these converge on cotranscriptional mechanisms involving antisense transcripts (named *COOLAIR*) and different chromatin pathways (*3*, *4*). One of these pathways is vernalization, when prolonged cold increases *COOLAIR* transcription and induces a Polycomb-mediated epigenetic silencing of *FLC* (*5*, *6*). Another is the autonomous pathway, which involves alternative processing of *COOLAIR* transcripts that causes gene body histone K4 demethylation and *FLC* down-regulation (*4*, *7*). Because these regulators are conserved through evolution, *COOLAIR* regulation may have the potential to inform long noncoding RNA (lncRNA) function generally (*8*, *9*).

To investigate *COOLAIR* regulation, we undertook a forward mutagenesis screen using a luciferase reporter system (*pCOOLAIR:Luc*) (fig. S1) (*3*). *eoc1* (*enhancer of COOLAIR1*) was identified and mapped to a 32,000–base pair (bp) region on chromosome 4 (Fig. 1A and fig. S2, A to D). A G-A transition was detected in the ninth exon of At4g03090 that resulted in a premature stop codon (TGG to TGA). Complementation and allelic analysis confirmed that the enhanced Luc signal in *eoc1*-1 was due to the mutation of At4g03090 gene, previously named *AtNDX* (fig. S3, A to C) (*10*).

AtNDX is an atypical and highly divergent plant homeodomain (HD)–containing protein conserved in moss, *Selaginella*, and other flowering plants (Fig. 1B and fig. S4) (*10*). Analysis of insertion mutants (*eoc1*-2, *eoc1*-4) showed that AtNDX represses endogenous *COOLAIR* expression (Fig. 1, B and C). Relative to wild-type plants, the *eoc1*-2 and *eoc1*-4 mutants flowered later (fig. S5B) and their *FLC* expression was up-regulated (fig. S5C). The defect in *COOLAIR* expression was rescued by expression of FLAG-tagged AtNDX (fig. S6). AtNDX is expressed predominantly in dividing tissues such as young leaves, root tips, flower buds, and embryos (fig. S7).

The presence of the HD domain (Fig. 1B and fig. S4) and the localization of green fluorescent protein–tagged AtNDX in the nucleus and nucleolus (fig. S7C and fig. S8) prompted us to test whether AtNDX associates with *FLC* chromatin. Chromatin immunoprecipitation (ChIP) experiments using the FLAG-tagged AtNDX lines showed that AtNDX is enriched at the *COOLAIR* promoter–*FLC* terminator region (Fig. 2A). This suggests that the effects of AtNDX on *COOLAIR* are direct. GmNDX, the homolog of AtNDX in soybean, shows DNA binding via its HD domain (*11*). However, HD proteins can also bind RNA (*12*). To test the binding properties of AtNDX, we performed electrophoretic mobility shift assay (EMSA) analysis using a glutathione *S*-transferase (GST) recombinant protein that included the HD and NDX-B domain (GST-AtNDX; Fig. 1B and fig. S9A). We did not see binding of GST-AtNDX to double-stranded DNA (dsDNA) probes (Fig. 2B and fig. S9), but GST-AtNDX bound single-stranded DNA (ssDNA) in a non–sequence-specific manner (Fig. 2B, fig. S9D, and table S1). No binding to ssRNA, dsRNA, or RNA-DNA hybrids was detected (Fig. 2B, fig. S9, D and E, and table S1).

Single-stranded DNA can be formed in vivo during transcription if nascent RNA transcripts invade the dsDNA and anneal to the template strand in the duplex, generating an RNA-DNA hybrid. A three-stranded nucleic acid structure formed by an RNA-DNA hybrid plus a displaced ssDNA strand is called an R-loop (*13*). R-loops have been considered as transcriptional

[1]Department of Cell and Developmental Biology, John Innes Centre, Norwich Research Park, Norwich NR4 7UH, UK. [2]Sir William Dunn School of Pathology, University of Oxford, Oxford OX1 3RE, UK.

*Corresponding author. E-mail: caroline.dean@jic.ac.uk